Enhanced Fuzzy Tungsten Growth in the Presence of Tungsten Deposition

Patrick McCarthy[1], Dogyun Hwangbo[2], Matthew Bilton[3], Shin Kajita[4] and James W. Bradley[1]

[1] Department of Electrical Engineering and Electronics, University of Liverpool, Brownlow Hill, Liverpool, L69 3GJ, UK

[2] Graduate School of Engineering, Nagoya University, Furo-cho, Nagoya 464-8603, Japan

[3] Imaging Centre at Liverpool, University of Liverpool, Liverpool, L69 3GL, UK

[4] Institute of Materials and Systems for Sustainability, Nagoya University, Nagoya 464-8603, Japan

E-mail: `j.w.bradley@liv.ac.uk`

Abstract. Using a magnetron sputtering device operating in helium, fibre-form "fuzz" has been grown on tungsten samples in the presence of a significant auxiliary source of depositing tungsten. In this system, fuzzy tungsten was grown over a range of helium ion fluences, Φ_{He}, sample temperatures and helium ion energies, but with operator control over the tungsten atom-to-helium ion arrival rate ratio at the sample (from 0.003 to 0.009). In the presence of tungsten deposition, it appears that the fuzz growth has two distinct stages: at low to intermediate helium ion fluence the fuzzy layer thickness follows the expected $\sqrt{\Phi_{\mathrm{He}}}$ diffusive law augmented by approximately the "effective" thin film thickness of deposited tungsten; at high fluences the fuzz thickness increases very steeply with Φ_{He}. These observations are explained through the increase in the porosity of the fuzzy layer as it reaches thicknesses larger than $\sim 1\ \mu$m. It was observed that during the second phase of fuzz growth the thickness was highly dependent on both the sample temperature and the tungsten atom-to-helium ion arrival rate ratio. For the same helium ion exposure, an increase in the sample temperature from 1050 to 1150 K lead to a six-fold increase in the fuzzy layer thickness, whilst increasing the tungsten atom-to-helium ion arrival rate ratio over the full range produced a two-fold increase in the thickness. Microscopy and electron diffraction studies of the grown structures show clearly helium bubbles within polycrystalline tendrils.

Keywords: Helium, Fuzzy Tungsten, Magnetron Sputtering

Submitted to: *Nucl. Fusion*

1. Introduction

Tungsten will be used as a plasma facing material in the thermonuclear fusion device ITER [1] due to its unique properties namely; a high melting point, low sputtering yields on bombardment of plasma species and a low retention of hydrogen. However, during the operation of ITER, tungsten components will be exposed to high fluxes of helium ash, produced as a byproduct in the deuterium-tritium fusion reaction. Under certain surface temperature and helium ion fluence conditions, helium ion implantation leads to high pressure bubbles forming beneath the surface of tungsten [2, 3]. After sufficient helium plasma exposures (ion fluences $> 10^{24}$ m^{-2}) and high surface temperatures, the combination of helium bubble formation and plastic flow can produce tungsten fibre – form nanostructures known as fuzz [4]. The conditions for fuzz production have been well established through experiment; typically it requires helium ion bombarding energies $>$ 25 eV, surface temperatures in the range 1000 to 2000 K [5], and threshold helium ion fluences of $\sim$ 2 x 10^{24} m^{-2} [6]. The dependence of the fuzzy layer thickness, h, on the plasma exposure time, t, has been investigated in earlier work [7], and was shown to follow a diffusive law with:

$$\mathrm{h(t)} = (2\mathrm{Dt})^{\frac{1}{2}} \tag{1}$$

where D is the Fick's law diffusion coefficient for one dimensional material transfer. This relationship was subsequently recast by Petty et al [3] to be expressed in terms of helium ion fluence Φ_{He} (given by the product of the helium ion flux density Γ_{He} and exposure time t) as:

$$\mathrm{h}(\Phi_{\mathrm{He}}) = (\mathrm{C}(\Phi_{\mathrm{He}} - \Phi_0))^{\frac{1}{2}} \tag{2}$$

where Φ_0 is an experimentally determined incubation ion fluence, describing the threshold condition for fuzz formation. Here the constant C ($= 2\mathrm{D}/\Gamma_{\mathrm{He}}$) is dependent on the sample temperature, T_s, and has been calculated for a range of temperatures (1120 - 1400 K) in previous studies [7, 8, 9]. In practice, equation 2 can be used to predict the thickness of a fuzzy layer given the helium ion fluence and surface temperature reached during an experiment. Typically, one would expect for say surface temperatures of 1120 K, helium ion energies of 100 eV and fluences of 10^{25} m^2 a tungsten fuzz layer to have grown to a height of h $\sim$ 500 nm [6].

Recently, however, it has been found that fuzzy tungsten can grow at much higher rates than that predicted by equations 1 and 2 when helium ion irradiation is in the presence of tungsten deposition (for example from an external tungsten source) [10, 11, 12]. This may be important with respect to ITER's operation since a not insignificant flux of sputtered tungsten is expected to deposit on tungsten first wall components that are meeting the conditions (of temperature, helium ion fluence and ion energy) for fuzz to form [13, 14]. To simulate the effects of downstream deposition in a fusion reactor, Kajita *et al* exposed tungsten samples to deposition flux densities in the range 2.5 x 10^{18} - 1.75 x 10^{19} m^{-2} s^{-1} during fuzz growth in the NAGDIS II linear plasma device [10, 11]. The presence of this auxiliary tungsten source gave rise to super-fast growth rates of fuzz, producing millimeter-scale fuzzy structures on the irradiated tungsten surfaces. The produced tungsten morphologies were given the name Large Fuzzy Nanostructures (LFNs). In their findings, Kajita et al showed that for surface temperatures between 1200 and 1700 K and tungsten deposition flux densities between 2.5 x 10^{18} and 1.75 x 10^{19} m^{-2} s^{-1} LFNs could be formed [10]. In ITER, tungsten deposition flux densities (at tungsten plasma facing surfaces) are predicted to be around 0.4 – 1.1 x $10^{18}m^{-2}$ s^{-1} [13]. Despite these values being slightly lower than those used in [10, 11, 12] to observe LFN production, one may expect some enhancement in fuzz growth in ITER due to tungsten deposition.

In this study, through the use of a magnetron sputtering device, we are able to deposit tungsten atoms at a controlled rate on to tungsten samples as they transition to fuzz (through helium ion irradiation). Importantly, this is done with surface temperatures, helium ion energies and tungsten flux densities relevant to those expected at the ITER divertor [13, 14]. We study the effect of tungsten deposition on the growth rates and morphology of the resulting fuzz for helium ion fluences in the range of 4 x 10^{23} – 1 x 10^{25} m^{-2}. The magnetron grown fuzzy tungsten surfaces were compared and contrasted with those produced in a deposition-free environment of the linear plasma device NAGDIS II (across a similar ion fluence range). Our findings confirm previous studies that fuzz formation during deposition of tungsten results in significantly enhanced fuzz growth rates.

2. Experimental Arrangement

In this study, fuzzy tungsten samples were grown in two plasma systems, a magnetron sputtering source at the University of Liverpool and a magnetized linear plasma device (NAGDIS II) at Nagoya University. Both systems sustain DC helium plasmas as a source of ion irradiation; however the magnetron, by its nature, is equipped with a tungsten target cathode, capable of providing an auxiliary source of sputtered tungsten atoms for in situ deposition on the growing fuzzy layer. As described later, tungsten flux densities Γ_w at the sample up to a maximum of $\sim 10^{18}$ m^{-2} s^{-1} were produced. NAGDIS II is considered to be deposition-free. A summary of the operational parameters (helium ion flux density Γ_{He}, tungsten atom flux density Γ_w, helium ion energies E_{ion} and surface temperatures T_s) of the magnetron and NAGDIS II systems (as well as those predicted for the ITER divertor) are shown in table 1. A more thorough description of the magnetron and NAGDIS II, as well as the tools used for sample analysis, is given below.

2.1. Magnetron Sputtering Device

The magnetron sputtering system consisted of a V-Tech™ 150 unbalanced planar magnetron source housed in a 100 litre stainless steel chamber (both supplied by Gencoa Ltd). The magnetron was equipped with a 6” diameter x 0.25” thick tungsten target (purity 99.95 %) for sputter deposition. The vessel was pumped by the

Table 1: A comparison of the experimental parameters for the magnetron and NAGDIS II plasma devices, with the expected conditions within the ITER divertor [13, 14] also included.

Device	T (K)	E_{ion} (eV)	Γ_{He} (m^{-2} s^{-1})	Γ_{w} (m^{-2} s^{-1})
UoI Magnetron	1050 - 1150	80 - 100	1 x 10^{20}	3.0 - 9.4 x 10^{17}
NAGDIS II	1200 - 1220	70	5 x 10^{21}	——
ITER	300 - 1200	1 - 100	$\sim 10^{21}$	0.4 - 1.1 x 10^{18}

combinations of a 1000 l/s turbo-molecular pump (Leybold) backed by a rotary pump (Edwards EM240) providing an ultimate base pressure of 6.67 x 10^{-4} Pa. Through manipulation of a butterfly valve situated between the chamber and the pumping system the base pressure could be raised from 6.67 x 10^{-4} to 5.33 x 10^{-3} Pa. Helium gas (purity of 99.996 %) was supplied to the chamber through a mass flow controller (MKS Instruments), and the operating helium plasma pressure was measured by a capacitance manometer gauge (Type 627 MKS Instruments) to be 2.67 Pa. During operation, the DC plasma power was maintained at 700 W with a voltage of 300 V and a current of 2.4 A applied to the magnetron target. More details on the experimental apparatus are described in reference [6].

Tungsten sample discs (99.95 % purity) of 10 mm diameter and 1 mm thickness (supplied by Future Alloys) were positioned on the centre line of the system 100 mm downstream (and facing) the magnetron target, held in place by a housing incorporating an electron beam heater to bring the samples to working temperatures up to 1150 K. The samples were electrically biased (by a DC power supply) to provide ion bombarding energies between 80 and 100 eV. The sample temperatures were measured using an IR pyrometer (Micro-Epsilon UK Ltd, wavelength = 2.3 μm) situated outside the vessel and viewed via a vacuum window, with the emissivity of the tungsten samples determined to be 0.3.

Assuming sputtered W atoms leave the magnetron target with half the surface binding energy, equivalent to 8.68 eV [15], and the ionisation rate coefficient is $\sim$ 3 x 10^{-13} m^3 s^{-1} at an electron temperature of 8 eV [16], the mean free path of sputtered W atoms was 1.68 m at the plasma density 5 x 10^{15} m^3. As the distance between the tungsten samples and the magnetron target was around 100 mm it is likely that the samples were exposed to a majority of tungsten atoms and not ions in the experiments here.

Langmuir probe measurements carried out at the sample position showed that at our chosen operating chamber pressure (2.67 Pa) and discharge power (700 W) the electron density and temperature were 5 x 10^{15} m^{-3} and $\sim$ 7 eV respectively. From ion saturation current measurements with the probe we determined that over the ion energy range used in this study the helium flux density (Γ_{He}) was of the order 1 x 10^{20} m^{-2} s^{-1}. With plasma – sample exposure times up to 23 hours, helium ion fluences

Φ_{He} up to 10^{25} m^{-2} were achieved.

2.2. NAGDIS II

The linear magnetized plasma device NAGDIS-II (NAGoya DIvertor Simulator) was used to produce fuzzy tungsten samples in a deposition-free environment [17]. It consists of a high density helium plasma arc injected in a 0.1 T axial magnetic field. The system was pumped by two 2000 l/s turbo-molecular pumping systems (TG200M Osaka Vacuum Ltd) to achieve a base pressure of 1 x 10^{-5} Pa ($\sim$ two orders lower than the base pressure achievable in the magnetron system). The plasma operating pressure was chosen to be 0.67 Pa, regulated using a mass flow controller (HORIBA STEC), and measured using a capacitance manometer gauge (Type 627 MKS Instruments) located in the downstream region of the sample position.

Square tungsten samples (purity 99.95%) with sides of 10 mm length and 0.2 mm thickness were suspended on a conducting rod 1.4 m downstream of the plasma source, with the normal to their surfaces orientated parallel to the magnetic field lines. Samples were biased negatively, using a DC power supply, to maintain incident ion energies of 70 eV. The plasma itself (through particle bombardment) was used to heat the tungsten samples in the range 1200 - 1220 K. The surface temperatures were measured using an infra-red pyrometer (KTL-PRO), sensitive to 1.6 μm wavelengths.

Langmuir probe measurements close to the sample position had revealed typical electron density and temperature values of 7 x 10^{17} m^{-3} and $\sim$ 5 eV respectively, providing incident helium ion flux densities (Γ_{He}) of 4.7 x 10^{21} m^{-2} s^{-1}. Over plasma - sample exposure times of tens of minutes, helium ion fluences of 3 x 10^{24} - 1 x 10^{25} m^{-2} were produced.

2.3. Residual Gas Analysis (on the magnetron system)

A residual gas analysis (RGA) was performed using the Optix spectrometer (Gencoa Ltd) to obtain relative concentrations of impurity species (air species) inside the magnetron vacuum chamber, for a variation of base pressures from 6.67 x 10^{-4} to 5.33 x 10^{-3} Pa. The technique is based on the production of an optical emission spectrum using a remote plasma discharge. Spectra were obtained at each base pressure in the vacuum chamber prior to operation of the magnetron plasma.

2.4. Deposition Rate Measurements (in the magnetron system)

To obtain the deposition rate of tungsten sputtered from the magnetron target, a quartz crystal microbalance (QCM) with a gold foil was used. It was positioned 150 mm from the magnetron and thickness readings were recorded manually from a digital readout (Maxtek TM-400) over 45 minutes of plasma operation. The data yielded deposition rates for the two different base pressures chosen in the study. In the low density DC magnetron, it is assumed that the deposition flux consisted mostly of sputtered tungsten atoms, with a low proportion of plasma post-ionized metal species

[18, 19, 20]. Ionized impurity air species in the plasma are deemed to be responsible for the sputtering of the tungsten magnetron target, since sputter rates due to helium bombardment are known to be very low [21].

2.5. Fuzzy Tungsten Surface Microscopy

Surface analysis was performed on tungsten fuzz samples using a FEI Helios Nanolab 600i focused ion beam scanning electron microscope (FIB-SEM). A gallium ion beam milled and polished surface cross-sections, which were then imaged and measured to obtain fuzzy layer thicknesses. For each sample, protective coating layers of carbon and platinum were first deposited on the fuzzy surface and then length cross-sections of approximately 30 μm were milled out. Each FIB-SEM cross sectional image was taken at a tilt of 52° so to read exact lengths, image scale bars should be multiplied by a factor of $1/\sin(52°)$. To gain high-resolution information of the fuzzy structures, a lamella for S/TEM analysis was prepared using FIB milling and analysed using a JEOL 2100F Cs-corrected (200 kV) analytical FEG scanning/transmission electron microscope (S/TEM). Crystallographic information was obtained through selected area electron diffraction (SAED) and coupled with imaging by TEM, bright-field (BF) STEM and high-angle annular dark-field (HAADF) STEM.

3. Results and Discussion

Figures 1 a) and b) show RGA spectra for the two chosen base pressures of 6.67 x 10^{-4} and 5.33 x 10^{-3} Pa. The main species identified are those derived from air (e.g. N_2, O, O_2, H and OH). With an increased base pressure, the main N_2, O and O_2 peaks increase in intensity by five or six times, consistent with an eight fold increase in the backing pressure. These species are considered the main species that can sputter the magnetron target.

Figure 2 shows the thickness of tungsten thin films produced in the system (helium pressure of 2.67 Pa and discharge power of 700 W) for the two different base pressures cases as a function of time (for a 45 minute exposure). For these plots, we can calculate respective deposition rates of 17 ± 5 nm/hr and 54 ± 4 nm/hr. Since the plasma operating pressure was the same in each case, the three-fold increase in deposition rate at the higher backing pressure can be attributed to extra sputtering of the magnetron target due to an increased concentration of heavy air impurities. To help us make a clear comparison with the deposition conditions expected in ITER (see table 1), these deposition rates can be converted to a tungsten atom bombarding flux density, Γ_w, assuming a thin film density of 19,250 kg m^{-3} corresponding to a fully dense coating. We know from previous reports that thin films of tungsten produced by DC magnetron sputtering can have densities which are a few percent less than the density of bulk tungsten [22, 20]. In our calculation for Γ_w we ignore the small difference between bulk and thin film densities, assuming that the deposited tungsten layers produced on the QCM have densities consistent with bulk tungsten.

In figure 2, we have also plotted the tungsten atom fluence, equivalent to the product of Γ_w and the measurement time in seconds. For the two base-pressure cases we have Γ_w = 3.0 x 10^{17} m^{-2} s^{-1} and 9.4 x 10^{17} m^{-2} s^{-1} respectively. These are less than 1 % of the bombarding helium ion flux Γ_{He} ($\sim$ 1 x 10^{20} m^{-2} s^{-1}), yielding effective tungsten atom-to-helium ion arrival rate ratios Γ_w/Γ_{He} of 0.003 to 0.009. To confirm the QCM results, tungsten samples were weighed before and after tungsten deposition, allowing us to calculate the deposition rate to each sample. Our findings indicate that from the mass increase measured for each sample, a deposition rate consistent with the QCM measurements was made to these tungsten samples during the plasma exposure.

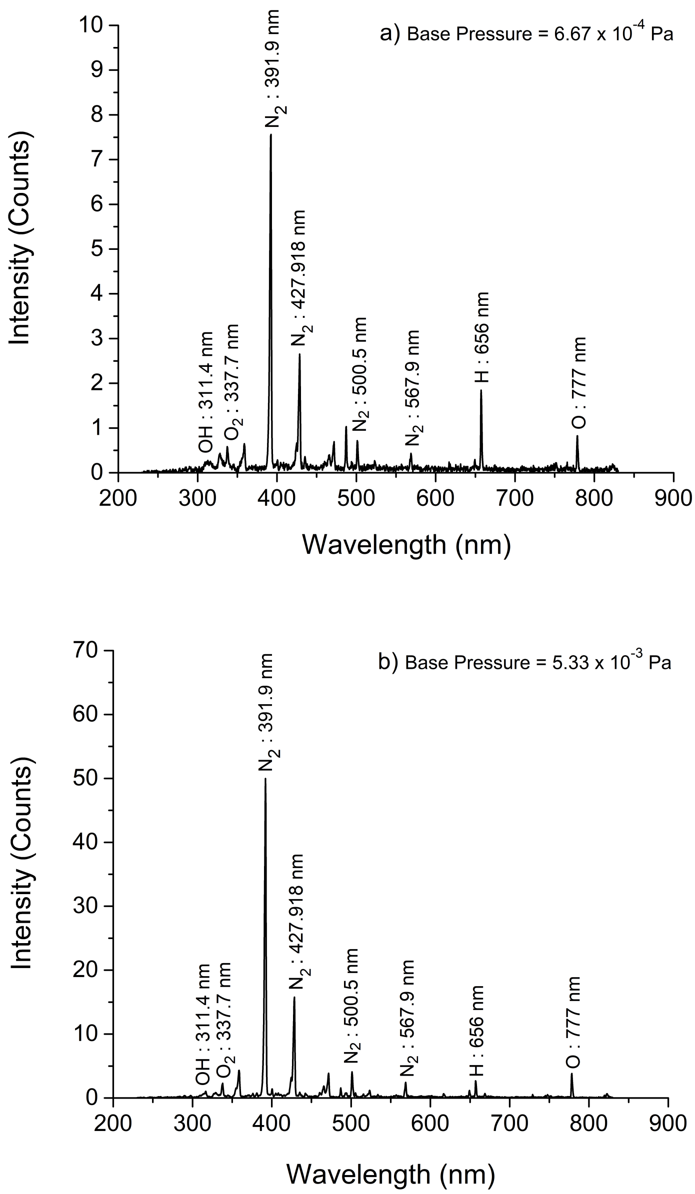

Figure 1: RGA (optical emission spectra) results obtained at the two base-pressures in the magnetron system for the two different base-pressures a) and b).

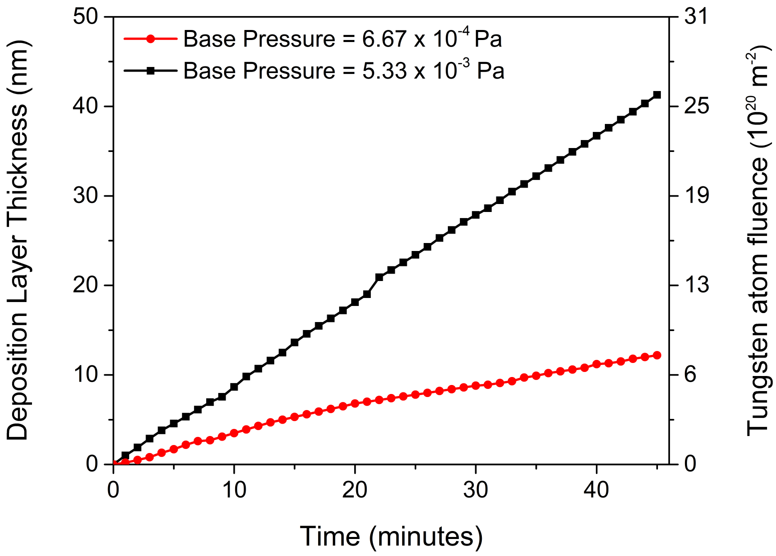

Figure 2: A plot of the tungsten deposition thicknesses and corresponding tungsten atom fluences versus time at the two chosen base pressures for an operating pressure of 2.67 Pa and plasma power of 700 W. In calculating the tungsten atom fluence a thin film density of 19,250 kg m^{-3}, corresponding to a fully dense coating of W, was assumed.

To compare fuzzy structures grown in deposition and non-deposition conditions, a combination of four SEM images of fuzzy layers produced in the magnetron and NAGDIS II for two different helium ion fluences ($\Phi_{\mathrm{He}} \sim 3 \times 10^{24}$ m^{-2} and $\sim 6 \times 10^{24}$ m^{-2}) and tungsten flux densities ($\Gamma_{\mathrm{w}} = 0$ and 9.4×10^{17} m^{-2} s^{-1}) are displayed in figure 3. The cross sectional SEM images in images figure 3 a) and c) were taken by first mechanically fracturing the fuzzy tungsten surfaces, allowing the cross section to be imaged. In the case of figures 3 b) and d), a protective layer of platinum has been deposited on to the fuzzy surfaces before ion beam milling was used to observe the cross section. The ion bombarding energies and surface temperatures were similar across the different experiments, being 70 eV and 1200 - 1220 K in the NAGDIS II and 80 eV and 1150 K in the magnetron system. It is clear from the images that a substantially thicker fuzzy layer is produced in the depositing system. The magnetron grown fuzzy tungsten, produced with simultaneous deposition of tungsten (shown in figures 3b) and d)) are roughly four times thicker than the corresponding layers produced with no deposition (in figure 3a) and c)). Close inspection of the fuzzy layer thicknesses in figure 3 reveals that, for these helium ion fluences, the difference in thickness between the depositing and non-depositing cases is greater than the thickness that a tungsten thin film would attain in non-fuzz conditions. For example, in the high ion fluence cases ($\Phi_{\mathrm{He}} = 6 \times 10^{24}$ m^{-2}), the fuzzy layer produced in NAGDIS II (figure 3c) has a thickness of 332 ± 68 nm, whereas that produced in the magnetron (figure 3d) is 1.17 $\pm$ 0.11 μm, the difference being 838 ± 189 nm. Over the $\sim$ 12 hours of exposure of the sample to the plasma in the magnetron, at a nominal deposition rate of 54 nm/hr, this would yield a 675 nm thin film, slightly less than the measured difference in the fuzz thickness of 838 ± 189 nm but similar when considering the error.

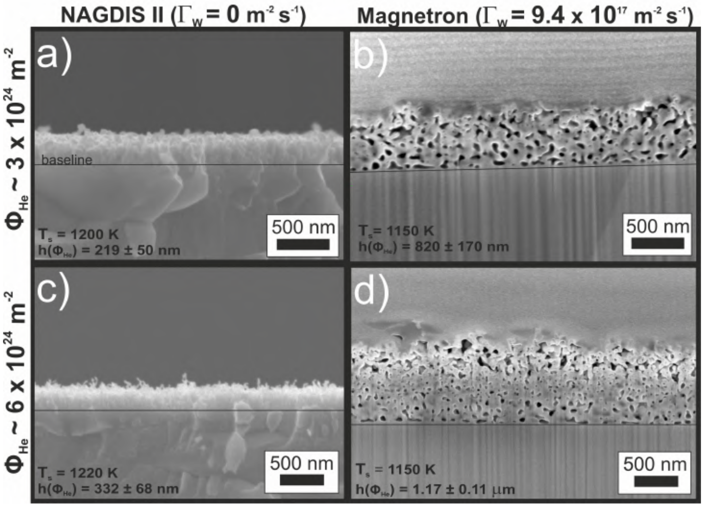

Figure 3: FIB-SEM cross-sectional images of fuzzy tungsten grown in deposition-free (a, c) and deposition (b, d) environments, for two different helium ion fluences. A black horizontal line laid over each image indicates the fuzz baseline. Samples in a) and c) are viewed by first mechanically fracturing the sample to access the cross section. Samples b) and d) are viewed at a 52 ° tilt angle.

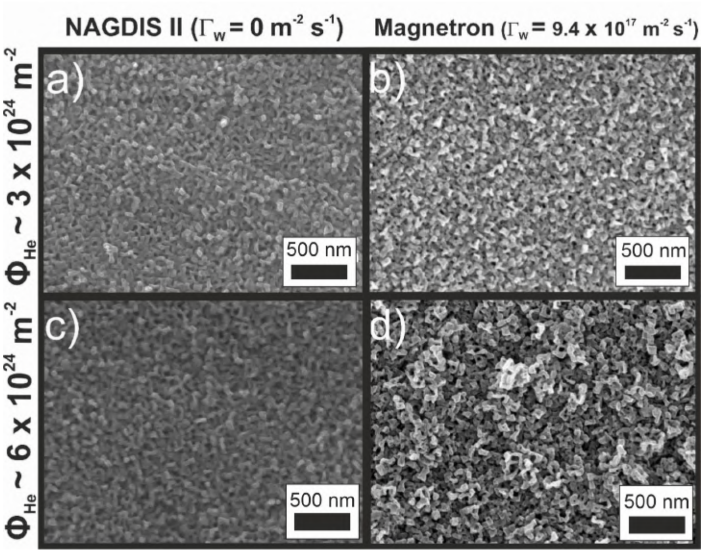

Figure 4: SEM images of the top of fuzzy tungsten surfaces grown in deposition-free (a, c) and deposition (b, d) environments, for two different helium ion fluences. The same four fuzzy surfaces that were used in the FIB-SEM cross sectional images of figure 3 are imaged here.

In figure 4 the SEM was used to image the top of fuzzy structures surface using the same four fuzzy samples as shown in figure 3. Interestingly, when the tendril diameters on each surface (figures 4a) to d)) are compared there is little difference to be found between those grown in deposition (figure 4b) and d)) and deposition free (figure 4a) and c)) environments. In both cases the tendril diameters was measured to be on the scale of tens of nanometres, this implies deposition does little to increase the width of tendrils but instead increases their height vertically from the surface.

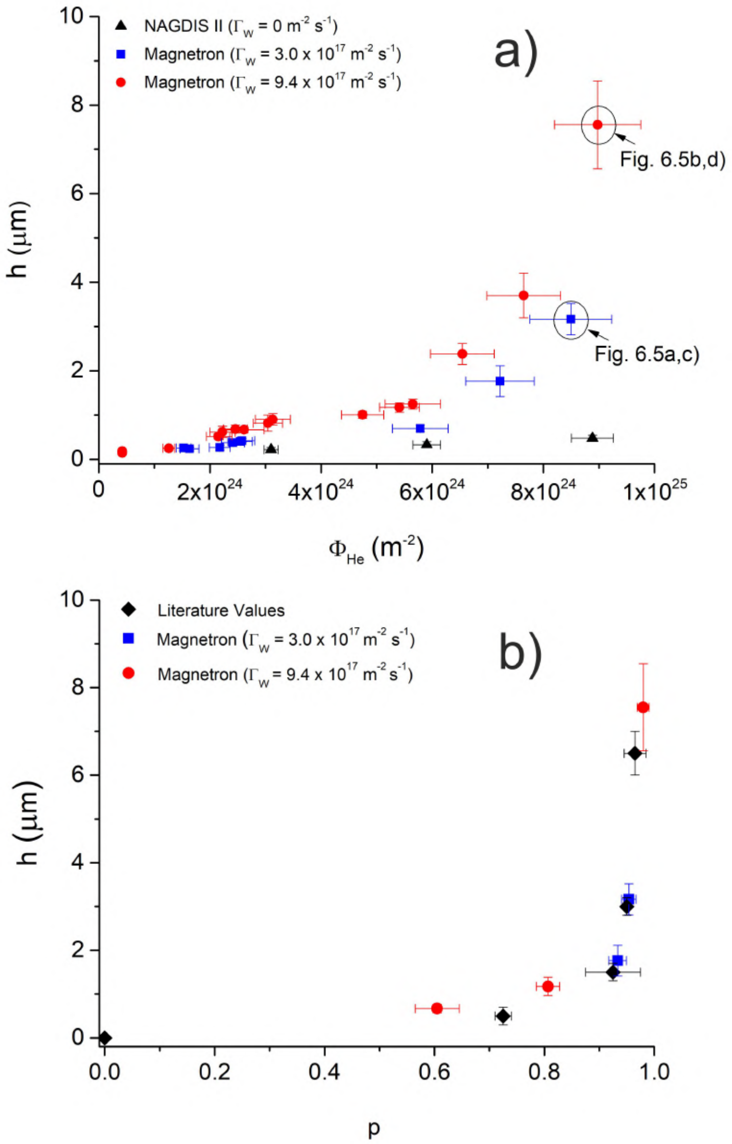

Figure 5: a) A plot of fuzz thickness versus helium ion fluence for each deposition flux density. b) a plot of fuzz thickness against the measured porosity of layers produced under each deposition flux density - included in this plot are porosity values from the studies in [6, 23].

To determine how the growth of the fuzzy tungsten layer is affected by a wider range of plasma exposures, samples were irradiated with helium ion fluences from 4 x 10^{23} to 9 x 10^{24} m^{-2} in the magnetron and NAGDIS II systems. In the case of the magnetron, fuzz growth was produced under tungsten deposition conditions with a tungsten atom flux density ranging from 3.0 x 10^{17} to 9.4 x 10^{17} m^2 s^{-1}. This was done for a range of surface temperatures from 1100 to 1150 K. Figure 5 a) shows the fuzzy layer thicknesses (h) over the range of helium ion fluences (Φ_{He}), in the different deposition conditions. Clearly, the presence of co-deposition of tungsten greatly increases the thickness h. In these cases, there appears to be two phases of fuzzy growth: at low to intermediate helium ion fluences (4 x 10^{24} m^{-2} $< \Phi_{\mathrm{He}} <$ 6 x 10^{24} m^{-2}) h is described by the expected growth in non-deposition conditions increased by an amount similar to the effective tungsten thin film layer that would be formed from tungsten deposition. At high fluences ($\Phi_{\mathrm{He}} >$ 6 x 10^{24} m^{-2}) h increases very steeply with Φ_{He} to produce fuzzy layers up to $\sim$ 8 μm in thickness.

In figure 5b) the porosity (p) of several fuzzy layers produced in the magnetron under each deposition flux density was measured. Using the mass difference before and after removing the fuzzy layer on the sample surface, a value for the porosity of each layer was calculated using the methods described in [23]. In total 5 samples were examined with each sample having an increasing fuzzy layer thickness. Also included in the data in figure 5b) are the values of porosity for fuzzy tungsten layers that have been calculated in previous studies [6, 23] across a fuzzy layer thickness range (0.5 - 6 μm). Note that a point is included in figure 5b) at a fuzz thickness of 0 μm to indicate a porosity of 0, as would be expected. Figure 5b) indicates that the porosity of the layers produced in the magnetron system increases as the layer thickness grows; this is consistent with previous observations of fuzzy layer porosity in the literature [6, 23].

In figure 5a) we would like to draw the reader's attention to the two largest fuzzy layers (indicated with black circles) that were produced for similar ion fluences (Φ_{He} $\sim$ 9 x 10^{24} m^{-2}) but different tungsten atom flux densities (Γ_{w} = 3.0 x 10^{17} m^{-2} s^{-1} and 9.4 x 10^{17} m^{-2} s^{-1}). By maintaining a helium ion fluence of $\sim$ 9 x 10^{24} m^{-2} and increasing the tungsten atom-to-helium ion arrival rate ratio ($\Gamma_{\mathrm{w}}/\Gamma_{\mathrm{He}}$) from 0.003 to 0.009, h increased by just over a factor of two (increasing from 3.17 $\pm$ 0.36 μm to 7.56 $\pm$ 1.00 μm). In figures 6 a) and b) the top surfaces for each layer are imaged to show the presence of interlocking fuzzy tendrils. In In figures 6 c) and d) FIB – SEM cross sectional imaging of these two particular layers shows clearly that a thicker fuzzy layer is grown under the larger deposition flux density condition.

3.1. Temperature Dependency on Fast Fuzz Growth

To better understand the effects of surface temperature on the onset of faster fuzz growth (circled cases in figure 5), additional fuzz surfaces (to those shown in figure 5) were grown in the magnetron under constant deposition conditions (Γ_{w} = 9.4 x 10^{17} m^{-2} s^{-1}) for helium ion fluences between 2 x 10^{24} and 1 x 10^{25} m^{-2} and a range of surface temperatures T_s between 1050 K to 1150 K. Figure 7 shows FIB - SEM images of four fuzzy samples with T_s equal to 1050, 1000, 1120 and 1150 K for the same helium ion fluence (Φ_{He} $\sim$ 9 x 10^{24} m^{-2}) and ion bombarding energy (100 eV). In figure 7 we see a large increase in the thickness of the fuzz layer from 1.32 $\pm$ 0.13 μm to 7.56 $\pm$ 0.39 μm for only a 100 K increase in T_s. This finding agrees well with previous reports where fuzzy tungsten layers were observed to grow at faster rates

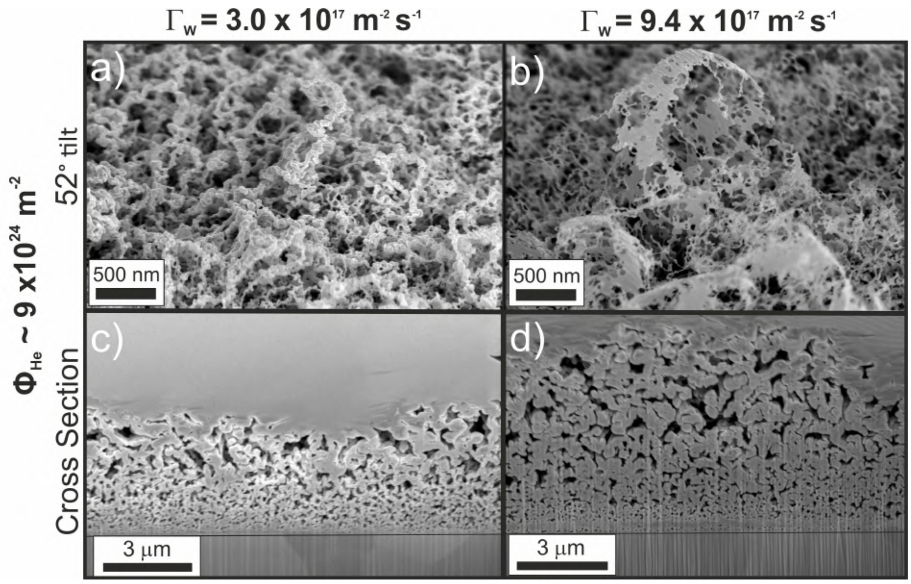

Figure 6: FIB-SEM images of the surfaces and cross sections fuzz samples grown for the same helium ion fluence of $\sim$ 9 x 10^{24} m^{-2}, surface temperature of 1150 K, and different tungsten deposition flux densities of a),c) 3.0 x 10^{17} m^{-2} s^{-1} and b),d) 9.4 x 10^{17} m^{-2} s^{-1}.

when the surface temperature was raised from 1120 K to 1320 K for a constant helium ion fluence [7]. To show clearly the two-phase growth of the fuzzy layer in deposition conditions and the dependency of surface temperature, it is convenient to plot the measured fuzzy layer thicknesses against ion fluence on a plot with log-log axes. This is done in figure 8 for Γ_w = 9.4 x 10^{17} m^{-2} s^{-1} together with data obtained in this study for deposition-free conditions on NAGDIS II, as well as previous data compiled by Petty *et al* on tungsten fuzz growth in deposition-free linear plasma devices [6]. In the study by Petty *et al*, the authors recorded the fuzz thicknesses produced for a range of helium ion fluences ($\sim$ 2 x 10^{24} to 1 x 10^{28} m^{-2}), sample temperatures (1100 - 1200 K) and ion energies (60 - 80 eV). These experimental conditions are similar to the conditions at which fuzz was grown in this present study, thus allowing a comparison to be made between the data sets. Inspection of figure 8 shows that in deposition-free conditions at low helium ion fluences ($\Phi_{He} < 3$ x 10^{24} m^{-2}) only small fuzzy thickness are obtained (h $\sim$ 5 x 10^{-2} μm), indicating that an incubation fluence is required

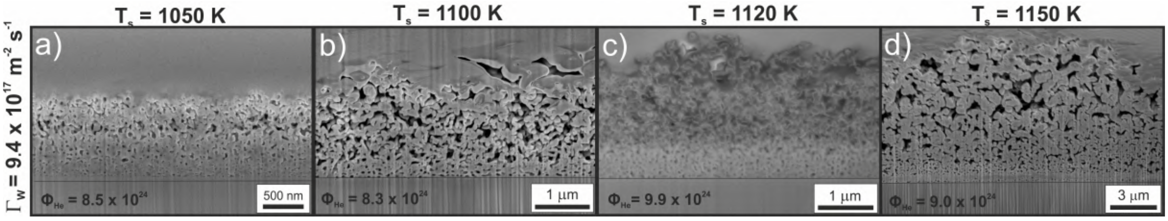

Figure 7: FIB-SEM cross-sectional images of fuzz grown in deposition conditions for a helium ion fluence of $\sim$ 9 x 10^{24} m^{-2} across a surface temperature range from 1050 to 1150 K.

to initiate fuzz growth. This behaviour can be represented by equation 2 (in section 1), in which the temperature-dependent constant C is found from a best fit from the deposition-free data (across the whole fluence range) to be 3.59 x 10^{-38} m^4 and with an incubation fluence Φ_0 = 2.5 x 10^{24} m^{-2} being appropriate. This relationship is shown as the dashed line in figure 8. However, this fit clearly does not hold for fuzzy surfaces grown with concurrent tungsten deposition (i.e. the magnetron data in figure 8), which shows significantly elevated growth rates between fluences of $\sim$ 2 and $\sim$ 6 x 10^{24} m^{-2} and super-fast rates above 6 x 10^{24} m^{-2}. In addition, we see evidence that increased surface temperatures lead to thicker fuzzy layers, as demonstrated by the data points around $\Phi_{He} \sim 10^{25}$ m^{-2} representing measurements at temperatures of 1050, 1120 and 1150 K. It is also clear that there is a much reduced incubation fluence when the initial stages of fuzz forms with deposition present. In this case, we can take $\Phi_0 \sim 0$ in equation 2, which is represented by the solid line in figure 8. It may be the case that an incubation fluence is still required in deposition conditions, however from this work Φ_0 would be less than the incubation fluence reported in [6] to be $\sim$ 2 x 10^{24} m^{-2}. It has been shown in previous studies that the early stages of fuzz growth can occur at fluences of close to 10^{23} m^{-2} [24, 25]. SEM imaging (not shown here) revealed that small fuzz-like nodules are present on the tungsten surface once a helium ion fluence of 4 x 10^{23} m^{-2} was reached, indicating fuzz-like structures can be observed at much lower fluences in the magnetron system.

Recently, the team of Kajita have observed very high growth rates of fuzz on tungsten surfaces exposed to helium ion irradiation and simultaneous tungsten deposition [10, 11, 12]. In [11], for a helium ion fluence Φ_{He} of 1 x 10^{25} m^{-2}, fuzzy layers grew to thicknesses of 100s of microns to several millimeters. By a way of comparison, in our own study we have observed a maximum fuzzy layer thickness of 8 μm for $\Phi_{He} \sim$ 1 x 10^{25} m^{-2}. The increased growth rate of fuzz in [11] relative to our own report is possibly due to the elevated range of surface temperatures and deposition flux densities used in [11]. Here, we have seen that increasing both the tungsten atom-to-helium ion arrival rate ratio Γ_w/Γ_{He} from 0.003 to 0.009 and surface T_s temperature from 1050 to 1150 K can lead to a two-fold and six-fold increase respectively in the fuzzy layer thickness. If we extrapolate to the experimental conditions in [11] (i.e T_s $\sim$ 1250 K, $\Gamma_w \sim$ 2.5 x 10^{18} m^{-2} s^{-1}, $\Phi_{He} \sim$ 1 x 10^{25} m^{-2}), and assuming the growth rate dependency for increases in Γ_w/Γ_{He} and T_s, we can estimate that fuzz thicknesses of $\geq$ 100 μm would be formed within our magnetron system. In future experiments, increasing the range of sample temperatures and deposition flux densities within the magnetron system should be investigated to confirm the scale of fuzzy structures that can be produced. A method to grow samples of fuzz with large thicknesses ($\geq$ 100 μm) would be useful, considering the applications of fuzz outside of fusion research, such as in photo catalysis [26] or water splitting for hydrogen production [27].

For the conditions in the ITER divertor, it is likely that where the thresholds for fuzz growth are met, increases in the tungsten atom-to-helium ion arrival rate ratio (Γ_w/Γ_{He}) and surface temperature could produce enhanced fuzz growth rates. Assuming the values in table 1, Γ_w/Γ_{He} is estimated to be in the range 0.0004 to 0.001

for ITER. This is roughly the same order of Γ_w/Γ_{He} that was sufficient to show an enhance fuzz growth rate in our own findings, which implies that a small enhancement in the growth rate of fuzz in ITER may occur. In addition, the estimated temperature range of the ITER divertor (300 - 2000 K) is not only sufficient to allow fuzz to grow in some areas, but will also mean that in the hottest regions of the divertor, much larger fuzz growth rates could be possible. Transient events, such as ELMs, can increase both the wall surface temperature and the tungsten deposition rate within a reactor, with deposition rates predicted to be five times larger during ELMs in ITER [13]. More recently it has been shown by De Temmerman *et al* that annealing due to the heat transfer during ELMs could ultimately negate fuzz growth completely if the surface temperature is high enough [28]. With this in mind, assuming lower surface temperatures than supposed annealing temperature of fuzzy tungsten ($\sim$ 1400 K [8]) are produced, there may exist a small temperature window where an ELM may not fully anneal away a fuzzy layer but raise the surface temperature so that enhanced growth rates can occur.

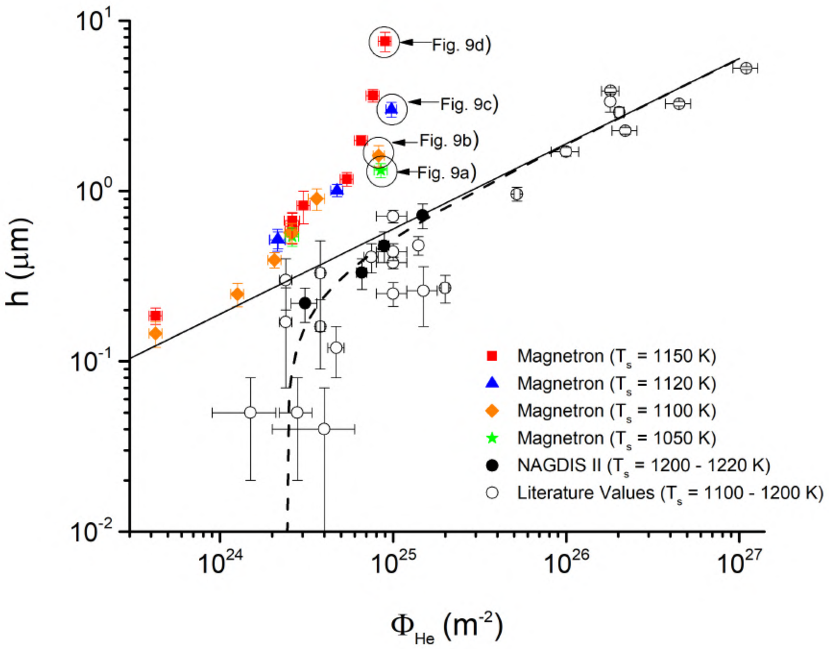

Figure 8: A log-log plot of the fuzzy layer thickness versus helium ion fluence for fuzz grown with simultaneous deposition (inside the magnetron) and in deposition-free conditions (inside NAGDIS II and from the literature [6]). The black dashed and solid lines represent analytical fits of the data to a diffusive growth law with and without an inferred incubation fluence respectively.

3.2. High Resolution Imaging of Magnetron Grown Fuzz

The Analysis by S/TEM was carried out by using the same magnetron fuzz sample as in fig.3b. The S/TEM images in fig.9 show the inner structure of the fuzzy tendrils formed on the sample's surface. Z-contrast in the HAADF images clearly shows porosity within the tendril structure, which is likely attributed to the presence of implanted helium bubbles, and bears a strong resemblance to previous HAADF imaging of fuzzy tendrils [29, 9, 30, 31]. Size variability of the implanted bubbles ranges from < 10 nm to 100 nm (approx.), and it is noticeable that the shape of the bubbles within the tendrils is varied, with no favoured bubble shape visible from the base toward the tip of a tendril, although larger bubbles tend to exist at the base. Larger helium bubbles are observed toward the base of the tendrils size of bubbles (size of ~ 50 nm) and smaller helium bubbles (5 nm average) are observed toward the tip (or top) of the tendril. This average size of 5 nm is consistent with the findings in [32] where the helium bubble diameter is estimated to be on average 4 nm when the helium incident ion energy is 50 eV.

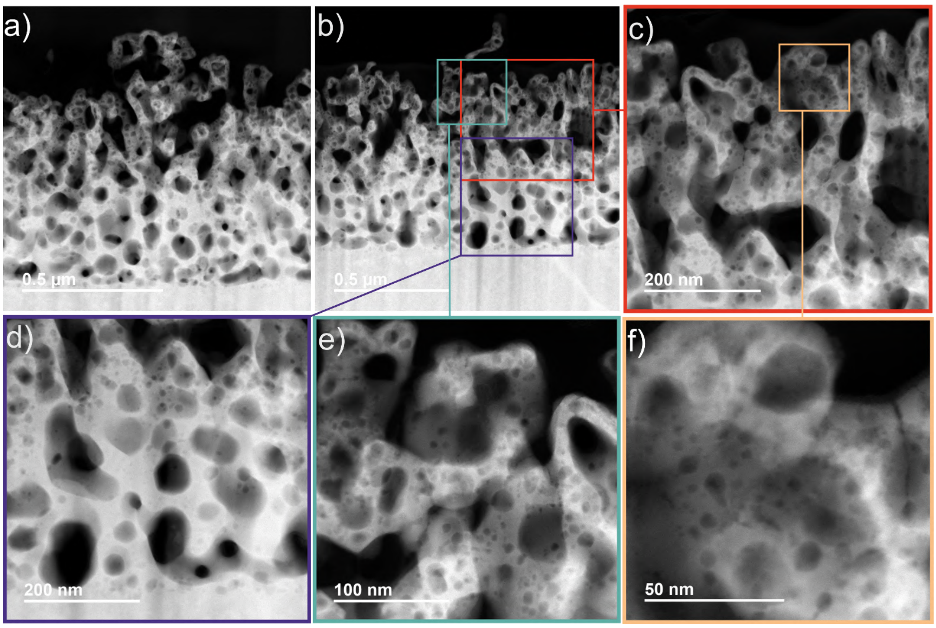

Figure 9: HAADF-STEM images (a) – f)) of the fuzz sample shown in figure 3b and 4b. Images a) and b) show low magnification images of the tendrils, and images c) - f) show magnified sections of the fuzzy layer shown in image b).

Crystallographic information of the same fuzzy sample was acquired through selected area electron diffraction (SAED) and is shown in figure 10. Three areas of interest were investigated; one from the bulk region of the sample where fuzz formation was deemed not to have occurred due to no visible helium bubble formation (figure 10b) – c)), and two from the fuzzy tungsten tendrils (figure 10d) – g)). In figure 10c) diffraction spots are attributable to single crystalline BCC tungsten [33]. Diffraction rings for the fuzzy tendril regions suggest more polycrystallinity in the structure (figure 10 e) and g)). Both fibril SAED patterns are also attributable to BCC polycrystalline tungsten, with common d-spacing's of 2.258, 1.597, 1.129, 1.010 Å. Some of the diffraction spots in figure 10e) and g) are attributable to FCC platinum, which originate from the protective surface layer deposited during FIB milling preparation.

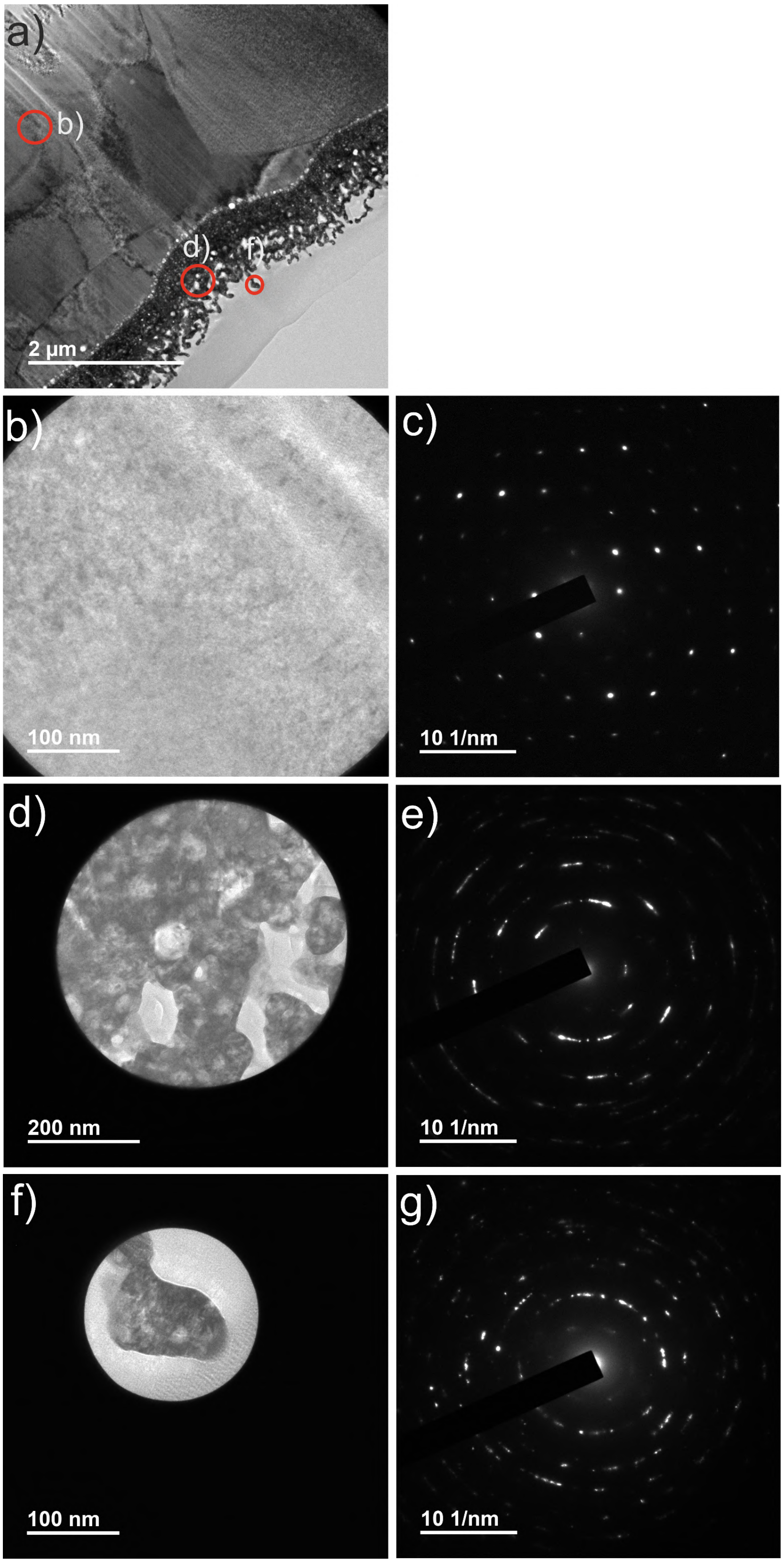

Figure 10: Cross-sectional TEM images and corresponding diffraction patterns, all produced using the same fuzz sample shown in figure 3b and 4b. Image a) shows a low magnification TEM image of the fuzzy surface cross-section. Images b), d) and f) are magnified regions as indicated on image a). Images c), e) and f) are the corresponding electron diffraction patterns produced from images b), d) and f) respectively.

3.3. Mechanisms For Enhanced Fuzz Growth

Currently, the exact growth mechanisms which produce fuzzy tungsten are unknown. It has been reported that fuzz forms due to helium diffusion and bubble growth beneath the surface in the early stages [34], with tungsten adatom diffusion [35, 36] or viscoelastic flows of tungsten [37] describing the later stages of its formation toward tendril growth. In experimental [6] and theoretical [37] studies, the fuzzy layer thickness was shown to follow a $\sqrt{\Phi_{\mathrm{He}}}$ growth law, implying diffusion processes govern the growth rate of the nanostructures. In the current study and reports by Kajita *et al* [10, 11, 12], it has been observed that when helium ion irradiation is coupled with tungsten deposition, the fuzzy layer thickness increases steeply with Φ_{He}. In [10] and [11], the authors described when the fuzzy layer thickness h is comparable to or greater than the plasma sheath thickness λ_s (i.e. h $\geq \lambda_s$), the sheath edge will not be flat but follow the shape of the fuzzy layer. As a result, an electric field would be formed around the tendrils, allowing helium ions to be captured by the grown structures, enhancing the rate of helium bubble creation.

In the current study, the sheath thickness at the sample surface within the magnetron system was calculated to be $\sim$ 50 μm, and in this regime (h $< \lambda_s$), the growing tendrils are unlikely to perturb the shape of the sheath, with therefore no enhancement in the ion capture. It is likely that the porosity of the layers produced in the magnetron can contribute toward the accelerated growth rate we observe when Φ_{He} $>$ 6 x 10^{24} m^{-2}. Referring to figure 5b) it is implicit that in the initial stages of fuzz growth ($\sim$ 4 x 10^{24} m^{-2} $< \Phi_{\mathrm{He}} < \sim$ 6 x 10^{24} m^{-2}), the porosity of the fuzzy layer can be considered small. Any tungsten deposition on these surfaces is, therefore, likely to form a close approximation to a thin film. As a result, measurements of the apparent fuzzy layer thickness will be augmented by this thin film layer when taken using the SEM, which appears to be the case. As the helium ion fluence to the surface increases ($\Phi_{\mathrm{He}} >$ 6 x 10^{24} m^{-2}), the fuzzy layer vertical height and porosity is increased. As we observe in figure 5 in the region where the fastest fuzz growth occurs, the porosity of the fuzzy layer is high ($>$ 80 %). In this case, tungsten deposition is likely to reach a porosity consistent with the surface it lands on. We can use the data in figure 5 a) and b) as an example. Approximately 14 hours of plasma exposure time was required to reach $\Phi_{\mathrm{He}} \sim$ 6 x 10^{24} m^{-2} and produce a fuzzy layer thickness of 1.5 μm. To increase $\Phi_{\mathrm{He}} \sim$ 9 x 10^{24} m^{-2} a further 7 hours of exposure is needed. In this time, a dense layer of tungsten deposition would have a thickness of $\sim$ 400 nm, given a deposition rate of 54 nm/hr. Assuming the surface porosity is now large (0.9), an additional layer of deposition with an equivalent porosity would lead to an increase of $\sim$ 4 μm in the layer thickness. This would result in a fuzzy layer thickness of around 5.5 μm, which is somewhat close to the measured fuzzy layer thickness of 7.56 $\pm$ 1.00 μm at 9 x 10^{24} m^{-2}. Clearly this is an estimation, but it may indicate a possible reason for the faster fuzz growth rate observed after $\Phi_{\mathrm{He}} >$ 6 x 10^{24} m^{-2} where the fuzzy layer porosity becomes very large.

4. Conclusions

In this study we have used a magnetron sputtering system, operating in helium, to grow fibre-form "fuzz" on tungsten samples with concurrent tungsten deposition. The fuzzy layers were grown over a range of helium ion fluences, Φ_{He}, (from 4 x 10^{23} to 1 x 10^{25} m^{-2}), sample temperatures, T_s, (from 1050 to 1150 K) and helium ion energies (from 80 to 100 eV). The system allowed operator control over the tungsten atom-to-helium ion arrival rate ratio, Γ_w/Γ_{He}, at the sample (from 0.003 to 0.009). In the presence of tungsten deposition, it appears that fuzz growth has two distinct stages: at low to intermediate helium ion fluences ($\sim$ 4 x 10^{24} m^{-2} $<$ Φ_{He} $< \sim$ 6 x 10^{24} m^{-2}) h follows $\sqrt{\Phi_{He}}$ augmented by the "effective" thin film thickness of deposited tungsten; at high fluences ($\Phi_{He} >$ 6 x 10^{24} m^2) h increases very steeply with Φ_{He}. These observations can be explained through the change in porosity of the fuzzy layer as it grows. In the low to intermediate ion fluence range ($\sim$ 4 x 10^{24} m^{-2} $<$ Φ_{He} $< \sim$ 6 x 10^{24} m^{-2}), fuzzy layers are much less porous. Therefore any increase in the fuzzy layer thickness in the presence of tungsten deposition will be comparable to the thin-film thickness of deposition. At higher ion fluence ($\Phi_{He} >$ 6 x 10^{24} m^2), fuzzy layers have larger thickness (h $>$ 1μm) and porosity (p $\sim$ 0.8 - 0.9). Thus, tungsten deposition would now coalesce with a highly porous surface leading to a more significant enhancement in the fuzzy layer thickness.

It was observed that the rate of growth in the second stage was dependent on both T_s and the tungsten atom-to-helium ion arrival rate ratio. For the same helium ion exposure ($\Phi_{He} \sim$ 9 x 10^{24} m^{-2}), raising T_s by 100 K from 1050 to 1150 K lead to a six fold increase in the fuzzy layer thickness, whilst increasing Γ_w/Γ_{He} from 0.003 to 0.009 produced a two-fold increase in the thickness. Microscopy and electron diffraction studies of the grown structures show helium bubbles present within polycrystalline tendrils. The magnetron results were compared directly with fuzzy tungsten layers grown in NAGDIS II, a deposition-free environment providing a similar range of ion fluences, ion energies and surface temperatures. Our comparisons show that under simultaneous tungsten deposition in the magnetron system enhanced growth rates of fuzz are produced. Our findings agree well with previous studies where enhanced growth rates can be attained through co-deposition of tungsten from an auxiliary source. On the likelihood of enhanced fuzz growth rates in ITER, our results show that if tungsten surfaces meet the conditions for fuzz growth, and this growth is coupled with some amount of tungsten deposition, the fuzz growth rate could be enhanced.

Acknowledgments

The authors would like to thank G. Blacoe and Dr. J. Brindley for their assistance in the investigation. P. McCarthy would like to gratefully acknowledge the Engineering and Physical Research Council (grant ref. EP/L01663X/1) for supporting this work.

5. References

[1] R. A. Pitts, S. Carpentier, F. Escourbiac, T. Hirai, V. Komarov, S. Lisgo, A. S. Kukushkin, A. Loarte, M. Merola, A. S. Naik, R. Mitteau, M. Sugihara, B. Bazylev, and P. C. Stangeby, "A full tungsten divertor for ITER : Physics issues and design status," *Journal of Nuclear Materials*, vol. 438, pp. S48–S56, 2013.

[2] H. Iwakiri, K. Yasunaga, K. Morishita, and N. Yoshida, "Microstructure evolution in tungsten during low-energy helium ion irradiation," *Journal of Nuclear Materials*, vol. 283-287, pp. 1134–1138, 12 2000.

[3] D. Nishijima, M. Y. Ye, N. Ohno, and S. Takamura, "Incident ion energy dependence of bubble formation on tungsten surface with low energy and high flux helium plasma irradiation," *Journal of Nuclear Materials*, vol. 313-316, no. SUPPL., pp. 97–101, 2003.

[4] S. Takamura, N. Ohno, D. Nishijima, and S. Kajita, "Formation of Nanostructured Tungsten with Arborescent Shape due to Helium Plasma Irradiation," *Plasma and Fusion Research*, vol. 1, pp. 051–051, 2006.

[5] S. Kajita, W. Sakaguchi, N. Ohno, N. Yoshida, and T. Saeki, "Formation process of tungsten nanostructure by the exposure to helium plasma under fusion relevant plasma conditions," *Nuclear Fusion*, vol. 49, no. 9, p. 095005, 2009.

[6] T. Petty, M. Baldwin, M. Hasan, R. Doerner, and J. Bradley, "Tungsten 'fuzz' growth re-examined: the dependence on ion fluence in non-erosive and erosive helium plasma," *Nuclear Fusion*, vol. 55, p. 093033, 9 2015.

[7] M. Baldwin and R. Doerner, "Helium induced nanoscopic morphology on tungsten under fusion relevant plasma conditions," *Nuclear Fusion*, vol. 48, p. 035001, 3 2008.

[8] S. Kajita, N. Yoshida, R. Yoshihara, N. Ohno, and M. Yamagiwa, "TEM observation of the growth process of helium nanobubbles on tungsten: Nanostructure formation mechanism," *Journal of Nuclear Materials*, vol. 418, no. 1-3, pp. 152–158, 2011.

[9] A. Khan, G. De Temmerman, T. W. Morgan, and M. B. Ward, "Effect of rhenium addition on tungsten fuzz formation in helium plasmas," *Journal of Nuclear Materials*, vol. 474, pp. 99–104, 2016.

[10] S. Kajita, S. Kawaguchi, N. Ohno, and N. Yoshida, "Enhanced growth of large-scale nanostructures with metallic ion precipitation in helium plasmas," *Scientific Reports*, no. August 2017, pp. 1–9, 2018.

[11] S. Kajita, S. Kawaguchi, N. Yoshida, N. Ohno, and H. Tanaka, "Morphologies of co-depositing W layer formed during He plasma irradiation," *Nucl. Fusion*, vol. 58, p. 106002 (9pp), 2018.

[12] S. Kajita, N. Yoshida, S. Kawaguchi, H. Tanaka, N. Ohno, D. Nagata, and M. Tokitani, "Growth of membrane nanostructures on W co-deposition layer," *Nuclear Materials and Energy*, vol. 18, pp. 339–344, 1 2019.

[13] K. Schmid, K. Krieger, S. W. Lisgo, G. Meisl, and S. Brezinsek, "WALLDYN simulations of global impurity migration in JET and extrapolations to ITER," *Nuclear Fusion*, vol. 55, no. 5, 2015.

[14] G. De Temmerman, T. Hirai, and R. A. Pitts, "The influence of plasma-surface interaction on the performance of tungsten at the ITER divertor vertical targets," *Plasma Physics and Controlled Fusion*, vol. 60, p. 044018, 4 2018.

[15] Y. Kudriavtsev, A. Villegas, A. Godines, and R. Asomoza, "Calculation of the surface binding energy for ion sputtered particles," *Applied Surface Science*, vol. 239, no. 3-4, pp. 273–278, 2005.

[16] L. Vainshtein, I. Beigman, P. Mertens, S. Brezinsek, A. Pospieszczyk, and D. Borodin, "Ionization of W atoms and W+ ions by electrons," *Journal of Physics B: Atomic, Molecular and Optical Physics*, vol. 44, no. 12, 2011.

[17] N. Ohno, D. Nishijima, S. Takamura, Y. Uesugi, M. Motoyama, N. Hattori, H. Arakawa, N. Ezumi, S. Krasheninnikov, A. Pigarov, and U. Wenzel, "Static and dynamic behaviour of plasma detachment in the divertor simulator experiment NAGDIS-II," *Nuclear Fusion*, vol. 41, no. 8, pp. 1055–1065, 2001.

[18] I. Petrov, A. Myers, J. E. Greene, and J. R. Abelson, "Mass and energy resolved detection of ions and neutral sputtered species incident at the substrate during reactive magnetron sputtering of Ti in mixed Ar+N 2 mixtures," *Journal of Vacuum Science & Technology A: Vacuum, Surfaces, and Films*, vol. 12, pp. 2846–2854, 9 1994.

[19] C. Christou and Z. H. Barber, "Ionization of sputtered material in a planar magnetron discharge," *Journal of Vacuum Science & Technology A: Vacuum, Surfaces, and Films*, vol. 18, pp. 2897–2907, 11 2000.

[20] I.-L. Velicu, V. Tiron, C. Porosnicu, I. Burducea, N. Lupu, G. Stoian, G. Popa, and D. Munteanu, "Enhanced properties of tungsten thin films deposited with a novel HiPIMS approach," *Applied Surface Science*, vol. 424, pp. 397–406, 12 2017.

[21] W. Eckstein, "Calculated Sputtering, Re ection and Range Values.," in *Max-Planck-Institut fur Plasmaphysik*, 2002.

[22] I. Prencipe, D. Dellasega, A. Zani, D. Rizzo, and M. Passoni, "Energy dispersive x-ray spectroscopy for nanostructured thin film density evaluation," *Science and Technology of Advanced Materials*, vol. 16, no. 2, p. 25007, 2015.

[23] D. Nishijima, M. J. Baldwin, R. P. Doerner, and J. H. Yu, "Sputtering properties of tungsten 'fuzzy' surfaces," *Journal of Nuclear Materials*, vol. 415, no. 1 SUPPL, pp. 96–99, 2011.

[24] T. Petty, A. Khan, T. Heil, and J. Bradley, "Fuzzy tungsten in a magnetron sputtering device," *Journal of Nuclear Materials*, vol. 480, pp. 374–385, 11 2016.

[25] F. W. Meyer, H. Hijazi, M. E. Bannister, K. A. Unocic, L. M. Garrison, and C. M. Parish, "Flux threshold measurements of He-ion beam induced nanofuzz formation on hot tungsten surfaces," *Physica Scripta*, vol. 2016, no. T167, 2016.

[26] S. Kajita, T. Yoshida, D. Kitaoka, R. Etoh, M. Yajima, N. Ohno, H. Yoshida, N. Yoshida, and Y. Terao, "Helium plasma implantation on metals: Nanostructure formation and visible-light photocatalytic response," *Journal of Applied Physics*, vol. 113, no. 13, p. 134301, 2013.

[27] M. de Respinis, G. De Temmerman, I. Tanyeli, M. C. van de Sanden, R. P. Doerner, M. J. Baldwin, and R. van de Krol, "Efficient Plasma Route to Nanostructure Materials: Case Study on the Use of m-WO 3 for Solar Water Splitting," *ACS Applied Materials & Interfaces*, vol. 5, pp. 7621–7625, 8 2013.

[28] G. De Temmerman, R. Doerner, and R. Pitts, "A growth/annealing equilibrium model for helium-induced nanostructure with application to ITER," *Nuclear Materials and Energy*, vol. 19, pp. 255–261, 5 2019.

[29] S. Kajita, N. Ohno, N. Yoshida, R. Yoshihara, and S. Takamura, "Arcing on tungsten subjected to helium and transients: ignition conditions and erosion rates," *Plasma Physics and Controlled Fusion*, vol. 54, no. 3, p. 035009, 2012.

[30] K. Wang, R. P. Doerner, M. J. Baldwin, F. W. Meyer, M. E. Bannister, A. Darbal, R. Stroud, and C. M. Parish, "Morphologies of tungsten nanotendrils grown under helium exposure," *Scientific Reports*, vol. 7, no. December 2016, pp. 1–9, 2017.

[31] K. Zhu, Y. Xing, T. Liu, R. Yang, Z. Long, H. Zhou, L. Luo, P. Zhou, X. Ye, W. Wang, and Y. Hu, "Studies of He irradiated tungsten using transmission electron microscope," *Materials Letters*, vol. 213, pp. 362–365, 2018.

[32] K. Wang, M. E. Bannister, F. W. Meyer, and C. M. Parish, "Effect of starting microstructure on helium plasma-materials interaction in tungsten," *Acta Materialia*, vol. 124, pp. 556–567, 2017.

[33] K. Lejaeghere, V. Van Speybroeck, G. Van Oost, and S. Cottenier, "Error Estimates for Solid-State Density-Functional Theory Predictions: An Overview by Means of the Ground-State Elemental Crystals," *Critical Reviews in Solid State and Materials Sciences*, vol. 39, pp. 1–24, 1 2014.

[34] F. Sefta, K. D. Hammond, N. Juslin, and B. D. Wirth, "Tungsten surface evolution by helium bubble nucleation, growth and rupture," *Nuclear Fusion*, vol. 53, no. 7, p. 073015, 2013.

[35] Y. V. Martynenko and M. Y. Nagel', "Model of fuzz formation on a tungsten surface," *Plasma Physics Reports*, vol. 38, no. 12, pp. 996–999, 2012.

[36] D. Trufanov, E. Marenkov, and S. Krasheninnikov, "The role of the adatom diffusion in the tungsten fuzz growth," *Physics Procedia*, vol. 71, no. February, pp. 20–24, 2015.

[37] S. I. Krasheninnikov, "Viscoelastic model of tungsten 'fuzz' growth," *Physica Scripta*, vol. T145, p. 014040, 12 2011.